06

The mechanical response of pre-strained [100] aluminium single crystals under plane impact

© G.V. Garkushin,[1,2] A.S. Savinykh,[1,2] S.V. Razorenov,[1,2] D.Yu. Rasposienko,[3] I.G. Brodova[3]

[1] Federal Research Center for Problems of Chemical Physics and Medical Chemistry, Russian Academy of Sciences, 142432 Chernogolovka, Moscow region, Russia
[2] Joint Institute for High Temperatures, Russian Academy of Sciences, 125412 Moscow, Russia
[3] M.N. Mikheev Institute of Metal Physics, Ural Branch, Russian Academy of Sciences, 620108 Yekaterinburg, Russia
e-mail: garkushin@ficp.ac.ru

Received July 17, 2023
Revised August 23, 2023
Accepted September 3, 2023

New data have been obtained on the resistance to high-strain rate and fracture of a [100] aluminum single crystal under plane impact loading. The evolution of the elastoplastic compression wave, the Hugoniot elastic limit, and the spall strength of samples in the states before and after pre-starined of 0.6%, 5.5%, and 10.5% were measured. Pre-strain was carried out by compression on a hydraulic press. Shock loading was carried out on an air gun with simultaneous recording of wave profiles ufs(t) using a VISAR laser interferometer. The maximum shock compression pressure did not exceed 4 GPa. It was found that pre-strain by 0.6% and the associated change in the defectiveness of the structure, changes the kinetics of deformation and reduces the value of the Hugoniout elastic limit. Increase in the amount of pre-strain to 5.5% and 10.5% leads to an insignificant increase in the Hugoniout elastic limit relative to the samples without deformation. The compression rate in a plastic shock wave does not depend on the state of single crystals. Pre-strain does not affect the spall strength. Based on the results of measurements, dependences of decay elastic precursor on the thickness of the samples and rate dependences of the spall strength were plotted in the range of 10^5-10^6 s^{-1}.

Keywords: Shock waves, structural defects, decay of elastic precursor, spall strength, wave profiles.

DOI: 10.61011/TP.2023.11.57497.181-23

Introduction

Elastic plastic properties of metals in shock waves depend to a great extent on the type of crystal lattice and orientation [1,2], collective behavior of the crystal structure defect assembly (twins, density of dislocations, lattice microstresses, point defects, etc.), amount of impurities, grainsize, texture, etc. Investigations of velocity dependences of strain and fracture resistance of prestrained aluminum and aluminum alloys are important for practical applications (light armor materials, aerospace structural components) as well as for building wide-range models and defining relations to calculate high-rate strain and fracture in extreme conditions [3]. Data obtained in the submicrosecond mechanical stress time range may be used to study the main patterns of structural factor effects [4–7]. Although industrial metals have polycrystalline structure, investigations of aluminum single-crystals [8–12] are crucial for understanding the main strain behavior in impact compression conditions, because for single-crystals, there is no influence of grain boundaries and process defects on their strain resistance. Great focus is made on the investigation of properties in quasistatic compression test [13–15] as well as in dynamic loading conditions [8,9], including using pre-preserved aluminum single-crystals after exposure to shock wave compression of various intensity [10–12]. Increase in dislocation density during preliminary impact compression of single-crystals results in strain hardening growth. The effect of dislocation density on dynamic response of metals are demonstrated in [16–18].

Over recent years, we have conducted a series of tests to examine the impact response of metals prestrained from 0.6% to 5% with hexagonal close-packed (HCP) lattice (molybdenum single-crystal [100] [19], titanium BT1-0 [20]) and body-centered cubic (BCC) lattice (armco-iron [21], vanadium [22]). Investigations have shown that sample prestrain and prestrain-induced change in density of mobile dislocations N_d change the strain kinetics dramatically.

The effect of relative low compression strain and strain-induced defects in aluminum single-crystals on the plastic strain kinetics, high-rate strain and submicrosecond load range fracture resistance are understudied. The existing aluminum single-crystal data require further investigation to supplement the existing data on the effect of microstructure defects on strain kinetics and plane impact load fracture mechanisms. The main objective of the study is to acquire new information on the shock wave evolution and mechanical response of aluminum single-crystals prestrained in order to change their microstructure state.

1. Materials and experimental

1.1. Preparation of the samples for impact tests

Experiments were performed on aluminum single-crystals with 99.99% purity and crystal-lattice orientation [100] prepared by the Bridgman method. Orientation was defined using the Laue patterns recorded on DRON-3 diffractometer, deviation from the set axis was not greater than 1°. Part of the samples were subjected to plastic deformation using the laboratory hydraulic press. The value of strain was nominally 0.6%, 5.5% and 10.5%. To assess the microstructure state parameters of the single-crystals, X-ray diffraction analysis (XDA) was carried out on the single-crystal samples using PANalytical Empyrean Series 2 laboratory diffractometer in $\lambda = 1.7902$ Å monochromatized CoK_α-radiation. Density of single-crystals was measured using the hydrostatic weighing method on ME204T („Mettler Toledo") analytical balance in automatic mode and was equal to $\rho_0 = 2.7 \pm 0.01$ g/cm^3. longitudinal speed of sound c_l was measured by ultrasonic method with converter frequency 2.5 MHz in all test samples. Shock wave test plane-parallel samples with the required orientation with a thickness from 0.2 mm to 4 mm were cut from a work piece using an electrical discharge machine.

1.2. Planar impact testing of the samples

Shock wave loading of samples was carried out using a setup consisting of a 50 mm air gun for impact compression pulse generation and interferometer VISAR [23]. Helium was used as working gas for all experiments. An interferometer was used for continuous recording of wave profiles — dependence of free surface velocity on time $u_{fs}(t)$ with high time and spatial resolution. For plane impact compression, the samples bumped against 0.1 to 1 mm flat aluminum (99.3%) plates with a velocity of $v_0 = 470 \pm 10$ m/s along crystallographic orientation [100]. The impact plates were mounted on a 5 mm polymethyl methacrylate (PMMA) substrate placed at the hollow aluminum shell end to avoid deflection during acceleration in the gun barrel. Velocity of impactor and angle to the sample plane before impact were controlled using four contact sensors. The gun barrel and the space around the sample were evacuated before the experiment.

2. Experimental results

2.1. Assessment of microstructure state of [100] aluminum single-crystal by the XDA method

Plastic uniaxial compression strain of aluminum single-crystals at room temperature develops by dislocation sliding. Dislocation density was assessed using averaged microstresses perpendicular to the exposed surface ε_{hkl} and sizes of the coherent scattering regions D derived from the analysis of Bragg peak profiles from various atomic planes. When the peak was separated into several peaks (typical for 5.5% and 10.5 % strained samples), the most intense peak was used for the analysis. Since the single-crystals were oriented with plane (100) parallel to the sample plane, to obtain reflections from planes (110), (111) and (311), the samples were rotated at 45.9°, 54.73° and 25.52°, respectively. The dislocation density was calculated using the following equation [24]:

$$N_d = \frac{2\sqrt{3}|\varepsilon_{hkl}|}{Db},$$

where ε_{hkl} are microdistortions perpendicular to the exposed plane (hkl), D are dimensions of the coherent scattering region, b is the Burgers dislocation vector for pure aluminum $b = 2.8631$ Å. CSR dimensions and microstresses were determined graphically by the Williamson-Hall method [25–27]:

$$\frac{\cos\theta}{\lambda} = \frac{0.9}{D} + 4\varepsilon\frac{\sin D}{\lambda},$$

where β is the Bragg peak broadening at half maximum, ε are microstresses.

Table 1 shows average parameter values obtained during XDA. Here, a is the lattice constant, Δa = pristine — pre-strain (%) is the pre-strain and post-strain lattice constant difference, $\langle\varepsilon^2\rangle^{1/2}$ are lattice microstrains, ε are microstrains, N_d are dislocation densities, c_l is the longitudinal speed of sound of aluminum single-crystals in orientation [100].

Table 1 shows that the initial and 0.6% strained samples have lattice constants that are close to pure aluminum ($a = 4.0488$ Å). Much larger changes take place after 5.5% and 10.5% strain. For 0.6% strain, Bragg peak offset was observed on the diffraction patterns. This is indicative of crystal lattice distortion due to elastic stresses. In addition, profile broadening was observed that was caused by the increase in concentration of disordered dislocation type defects that agrees with the analysis that showed slight increase in dislocation density (Table 1). Two competing processes occur at such types of strain. On the one hand, the number of dislocations is growing, that is clearly seen from the comparison of dislocation densities. The increasing number of defects results in broadening of peak profiles and their displacement from the ideal defectless position due to large amount of elastic stresses. On the other hand, generation of a large number of dislocations in case of 5.5% and 10.5% samples results in interaction between them with formation of ordered configurations, walls and sub-boundaries. Such interaction reduces microstresses and dislocation density (Table 1).

2.2. Elastic-plastic compression wave evolution in aluminum single-crystals [100]

Figure 1 shows impact compression test data for four types of 4 mm aluminum single-crystal samples. Impact compression pressure in all experiments was equal

Table 1. Microstructure state parameters of aluminum single-crystals [100]

Sample state	a, Å	Δa	D, Å	$\langle\varepsilon^2\rangle^{1/2}$	ε	$N_d \cdot 10^5$, cm^{-2}	c_l, m/s
Pristine 0%	4.04790	–	64	–	0.016217	9.2	6360
Pre-strain 0.6%	4.04679	0.00111	63	0.000438	0.016595	9.4	6316
Pre-strain 5.5%	4.05743	0.00953	103	0.002352	0.011439	7.0	6306
Pre-strain 10.5%	4.05935	0.01145	129	0.005225	0.009135	6.8	6287

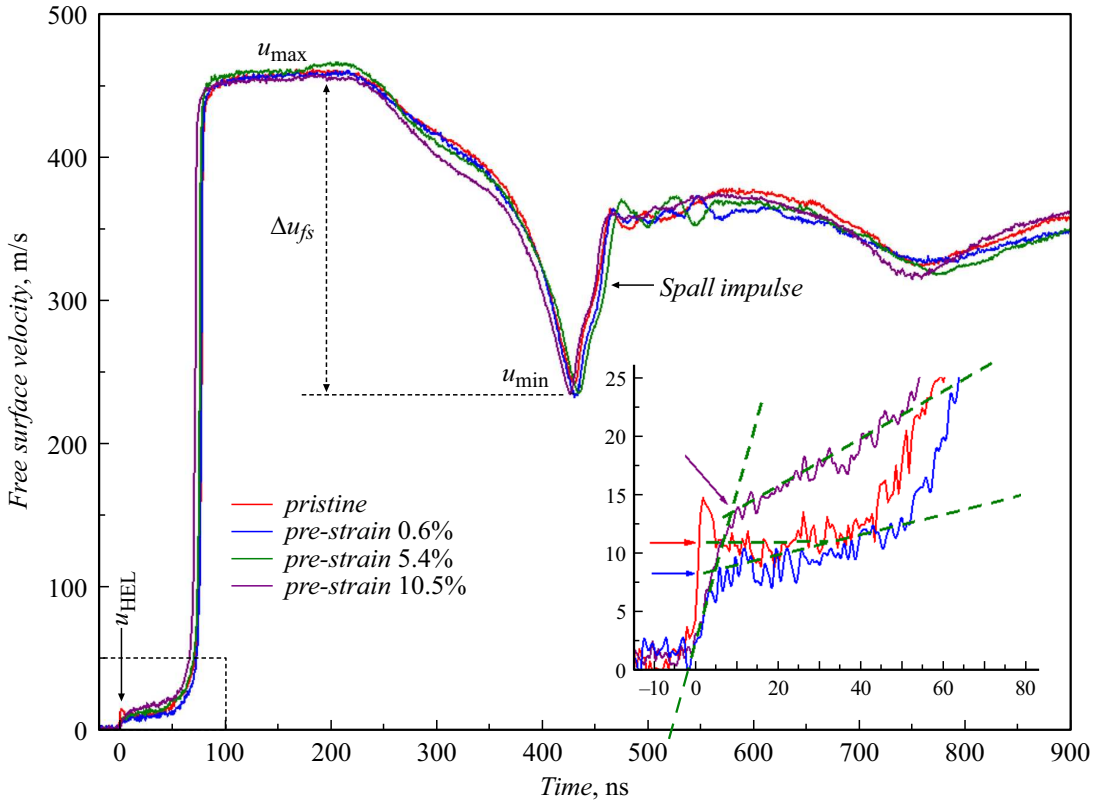

Figure 1. Free surface velocity profiles $u_{fs}(t)$ of aluminum single-crystals [100] before and after 0.6%, 5.5% and 10.5% strain. Nominal thickness of all samples was equal to 4 mm. The detail shows zoomed in frontal parts of the elastic-plastic transition. The place where elastic precursor amplitude was determined is marked with the dashed lines.

to 3.6 ± 0.1 GPa. On all wave profiles, exposure of elastic precursor with amplitude u_{HEL} is successively recorded on the impact compression sample, the precursor is followed by the plastic compression wave and parameter constancy region u_{max}, then, in turn, expansion wave propagates and reduces the surface velocity to the minimum value u_{min} associated with dynamic (spall) fracture of the material in this point of time. The parameter constancy duration is defined by the wave reverberation time in the impactor and, accordingly, the greater the duration the greater the impactor thickness.

The detail in Figure 1 shows zoomed in frontal parts of the wave profiles that demonstrate the prestrain effect on the precursor amplitude and shape. Ii was shown in [2] that aluminum deforms due to fast movement of dislocations, as a result, low elastic strength in impact loading conditions and fast (often exceeding the time resolution of diagnostic methods) growth of the finite impact amplitude are observed. Elastic precursor of a non-strained single-crystal contains a peak at the elastic compression wave front and, therefore, has parameters in the maximum and minimum point between the elastic and plastic waves. Peaks at the elastic precursor front and peak-induced stress release downstream of the precursor front are usually attributed to intensive generation (propagation) of plastic strain carriers (dislocations or twins) [28,29]. u_{HEL} value for initial Al single-crystal [100] agrees with the data obtained in [10] on 4.5 mm Al single-crystal [100] samples, where it was equal to 10.5 m/s. Post-strain change in the dislocation density by 0.6% results in disappearance of peak at the front and precursor amplitude decrease from 10.8 m/s to 8.3 m/s compared with the initial sample. After 5.5% and 10.5% prestrain, growth of amplitude u_{HEL} up to 11.4 m/s and 13.8 m/s, respectively, occurs.

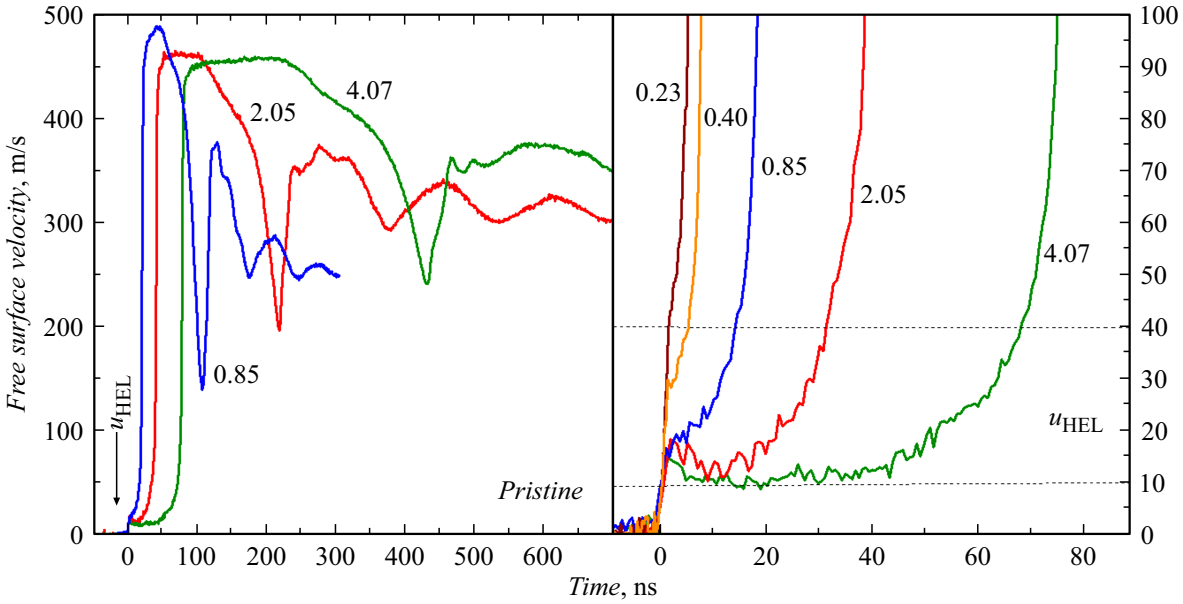

Figure 2. Free surface velocity profiles of aluminum single-crystals [100] in the pristine state. Zoomed in frontal parts of the elastic-plastic transition are shown on the right side. Numbers show the sample thicknesses in millimeters. Dashed lines in the figure show the minimum and maximum amplitudes of the elastic precursor depending on the sample thickness.

In the initial samples, the growth time in the elastic precursor was about 2.4 ns, while after 0.6% strain and higher — this time was from 7 ns to 13 ns. Comparison of wave profiles in single-crystals does not show any obvious change in the shock wave compression rate, that is indicative of a close dislocation density after slight plastic strain. Time of plastic shock wave exposure on the free surface in the described experiments is defined by the sample thickness and speed of sound. Parameter growth time in the plastic shock wave for all samples was about 5 ns.

Figures 2 and 3 show full free surface velocity profiles and frontal parts of aluminum single-crystals in initial state and after 10.5% strain depending on thickness. Compression stress downstream of the elastic precursor σ_{HEL} corresponding to the Hugoniout elastic limit of the material HEL is calculated as follows [30]:

$$\sigma_{HEL} = \frac{1}{2}\rho_0 c_l u_{HEL}. \quad (1)$$

Measurements of stresses behind of the precursor front in the aluminum single-crystal samples with various thickness are summarized in Figure 4.

The measurements demonstrate precursor decay during propagation in the sample due to the development of plastic strain directly downstream of the front. The maximum decay occurs in the initial and 0.6%strained single-crystal samples. Increase in the sample strain up to 5.5% and 10.5% results in reduction of the Hugoniot elastic limit decay rate. Dependences of the Hugoniot elastic limit on the single-crystal aluminum sample thickness in initial state and after prestrain that are shown in Figure 4 are approximated by the power function [28]:

$$\sigma_{HEL} = S(h/h_0)^{-\alpha}, \quad (2)$$

where S is the coefficient that becomes equal to σ_{HEL} at$h_0 = 1$ mm on the derived dependence, α is the power function index.

Table 2 summarizes coefficients S and power function index α for the tested single-crystal aluminum and literature data for pure aluminum and aluminum alloys is provided. The Table shows that α is very sensitive to structural defects. α found for 0.6% prestrained single-crystal decreases slightly compared with the initial single-crystal. For 5.5% and 10.5% prestrained samples, considerable reduction of the coefficient from 0.508 to 0.290 is observed. A similar effect was obtained also in [19] for a molybdenum single-crystal and is explained by the change in the dislocation motion mechanism. The obtained coefficients agree quite well with the literature data.

2.3. Spall strength of aluminum single-crystals [100]

Spall strength of materials in the extremely low load time region is analyzed by examining so-called „spallation“ phenomenon in compression pulse reflection from free surfaces of the body [30]. High-rate spall fracture is a kinetic process of initiation, growth and merging of multiple discontinuities. As a result of interference of the incident and reflected waves inside the body, tensile stresses are induced and may result in fracture, if they exceed the tensile strength of the material. The fracture is followed by stress relaxation, formation of two new free surfaces inside the

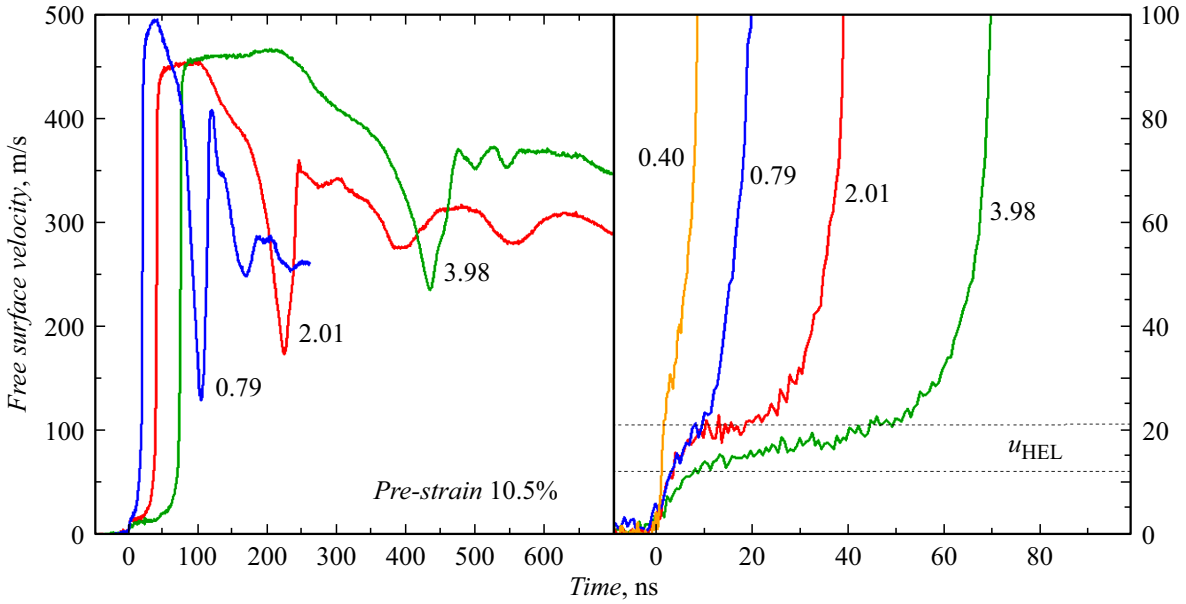

Figure 3. Free surface velocity profiles of aluminum single-crystals [100] after pre-strained 10.5%.

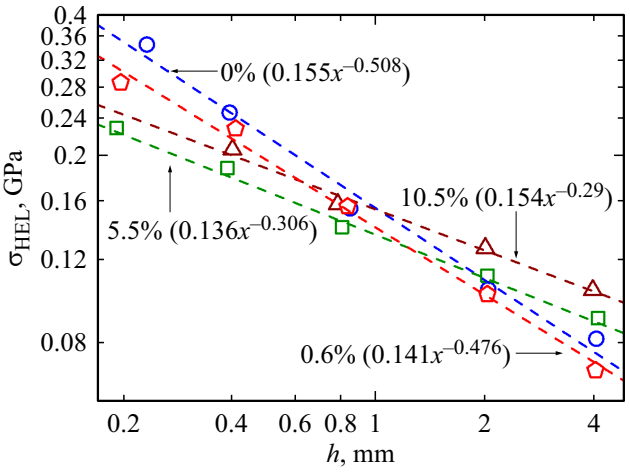

Figure 4. Decay of elastic precursor in aluminum single-crystals [100] depending on the initial state.

sample and occurrence of a compression wave on the wave profile, exposure of the compression wave on the surface initiates a spall pulse (Figure 1). Further surface velocity oscillations are caused by multiple wave reflections inside the separated sample layer between its rear surface and fracture surface. The oscillation period is defined by the spall plate thickness and speed of sound. The value of spall fracture stress in linear approximation is defined as [30]:

$$\sigma_{sp} = \frac{1}{2}\rho_0 c_b(\Delta u_{fs} + \delta u),$$

where $\Delta u_{fs} = u_{\max} - u_{\min}$ (Figure 1) is the so-called surface velocity decrement recorded using VISAR interferometer; c_b is the bulk speed of sound equal to 5120 m/s or all types of aluminum, δu is the allowance for velocity profile

Table 2. Coefficient S and power exponent α of the approximating function

State	S, GPa	α
Al 99.999% [28]	0.144	0.580
Al commercial[31–33]	0.155	0.535
6061 alloy[28]	0.133	0.364
Pristine 0%	0.155	0.508
pre-strain 0.6%	0.141	0.476
pre-strain 5.5%	0.136	0.306
pre-strain 10.5%	0.154	0.290

distortion due to the difference between the spallation pulse front velocity equal to c_l and the plastic component velocity of the upstream incident rarefaction wave moving with the bulk speed of sound (c_b) [34].

Wave profiles (Figure 1) of 4 mm aluminum single-crystals clearly show an elastic-plastic wave structure in unloading. Such behavior for aluminum single-crystals [100], [111] and [110] is thoroughly investigated in [11]. The authors point out the most pronounced quasielastic behavior for single-crystal [100], that is due to the maximum number of glide planes along orientation [100], which is 8 of 12 possible number. Simulation is [3] has shown that the number of active glide planes decreases when the sample compression increases in cold rolling. The profiles clearly show that the increase in the degree of strain effects the single-crystal behavior in unloading before fracture. spallation pulse slope (parameter growth time) is highly dependent on the fracture behavior. Figure 1–3 shows that aluminum single-crystal fracture occurs in a narrow region and is quite fast. Wave profiles from 0.8 to 4 mm samples

Table 3. Experiment conditions and measured strength properties of the pristine and pre-strained aluminum single-crystals [100]

Shots	State	h_{imp}, mm	h_s, mm	σ_{HEL}, GPa	σ_{sp}, GPa	$\dot{V}/V_0$, s^{-1}	h_{sp}, mm
1	0%	0.94	4.07	0.08	1.94	$2.50 \cdot 10^5$	0.99
2	0%	0.47	2.05	0.10	2.29	$5.10 \cdot 10^5$	0.49
3	0%	0.20	0.85	0.16	2.95	$12.5 \cdot 10^5$	0.24
4	0%	0.93	0.40	0.25	–	–	–
5	0%	0.94	0.23	0.35	–	–	–
6	0.6%	0.93	4.05	0.07	2.03	$2.70 \cdot 10^5$	0.99
7	0.6%	0.46	2.04	0.10	2.47	$5.80 \cdot 10^5$	0.50
8	0.6%	0.20	0.84	0.16	2.76	$11.6 \cdot 10^5$	0.23
9	0.6%	0.94	0.41	0.23	–	–	–
10	0.6%	0.93	0.20	0.29	–	–	–
11	5.5%	0.94	4.12	0.09	2.04	$2.70 \cdot 10^5$	1.00
12	5.5%	0.46	2.04	0.11	2.42	$4.90 \cdot 10^5$	0.51
13	5.5%	0.21	0.81	0.14	2.73	$12.3 \cdot 10^5$	0.23
14	5.5%	0.94	0.39	0.19	–	–	–
15	5.5%	0.94	0.19	0.23	–	–	–
16	10.5%	0.94	3.98	0.10	1.98	$2.50 \cdot 10^5$	0.99
17	10.5%	0.45	2.01	0.13	2.56	$6.00 \cdot 10^5$	0.51
18	10.5%	0.20	0.79	0.16	2.98	$11.3 \cdot 10^5$	0.23
19	10.5%	0.93	0.40	0.21	–	–	–

Note. h_{imp} is the impactor thickness, h_s is the sample thickness, σ_{HEL} is the Hugoniot elastic limit, σ_{sp} is the spall strength, $\dot{V}/V_0$ is the strain rate before tensile failure, h_{sp} is the spall plate thickness

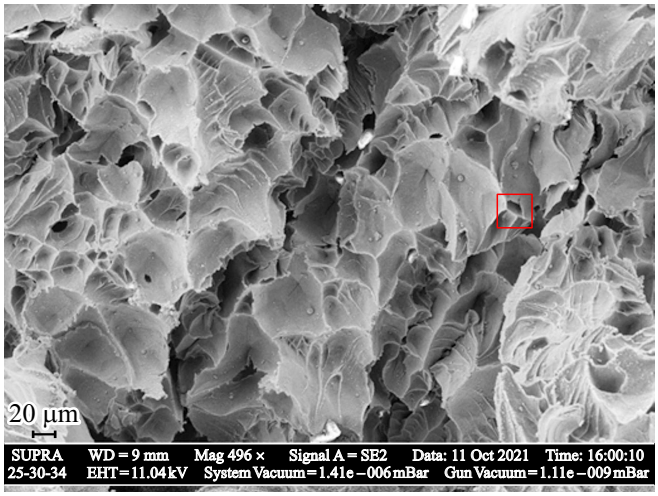

Figure 5. SEM image of the spall fracture zone. Square shows the cavity (pore) with sharp edges — spall initiation point.

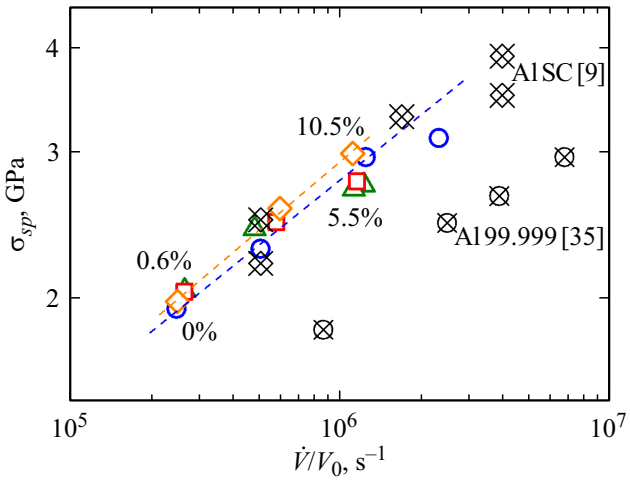

Figure 6. Measurements of spallation strength of aluminum single-crystal [100] depending on strain rate in the unloading wave. Empty circles are initial crystals, empty square, triangle and rhomb are 0.6%, 5.5% and 10.5% strained crystals, respectively. Crossed rhombs [9] data for single-crystals, crossed circles are data for high purity 99.999% aluminum [35].

show velocity growth time on the spall pulse front is from 10 ns to 30 ns. It should be noted that the single-crystal prestrain results in a slight growth of this time.

Fractographic analysis of the spallation surface was carried out on the 0.6% 2 mm single-crystal sample that drecovere the impact compression test. The analysis was performed using Zeiss SUPRA 25 field-emission scanning electron microscope (SEM) with resolution 1.7 nm at 15 kV. Figure 5 shows the aluminum single-crystal fracture surface. In our experimental conditions, spall fracture mechanism of aluminum is in nucleation, growth and merging of voids that are pores with approximately the same size and sharp edges in this case as shown in the images. Pore distribution in volume is rather uniform. The fracture surface has a network of crests and cup-shaped and tapered spherical recesses. Irregular-shaped cavities $20-30\,\mu$m in size that have formed after fast tension of the material are clearly shown. Such fracture behavior defines high single-crystal resistance to high-rate tension — high spall strength.

Figure 6 shows the dependence of spall fracture stress in aluminum single-crystals [100] in different states on

the strain rate. Here, the strain rate implies substance rarefaction in the expansion wave that is defined as follows

$$\frac{\dot{V}}{V_0} = -\frac{\dot{u}_{fsr}}{2c_b},$$

where $\dot{u}_{fsr}$ is the measured free surface velocity decrease rate of the test sample in the unloading component of the impact compression pulse. For comparison, the measured values are compared with the values for Al single-crystal [100] [9] and for high purity 99.999% aluminum [35].

The spall strength measurements of Al single-crystals [100] demonstrate fast growth with the increase in the tension rate and generally agree with the previously published data [9]. Figure 6 shows that both for the initial material and prestrained material, dependence of the spall strength on the strain rate is uniform, there is virtually no prestrain effect on the fracture stress variation. Pore growth behavior due to local shifts with formation of dislocation loops plays an important role in spall fracture [36]. Probability of occurrence of cavities on the defects is high. Growth of the defective structure in the volume shall result in considerable decrease in critical nucleus sizes and, thus, in nucleation energy gain that shall cause reduction of the spall strength. However, the spall strength is affected considerably by the presence of grain boundaries in high purity 99.999% aluminum, rather than by defect variation in the single-crystal.

Table 3 shows summarized experimental data and Hugoniot elastic limit measurements and spall strengths calculated on the basis of the experimental wave profiles.

Conclusion

Recording and analysis of full wave profiles were used to measure Hugoniot elastic limit and spall strength of the high purity aluminum single-crystal in the initial (non-strained) state and after 0.6%, 5.5% and 10.5% prestrain in impact compression in direction [100] of max. 4 GPa. For all types of single-crystal aluminum, Hugoniot elastic limit decay is observed independently of the degree of prestrain, whereby the decay rate decreases with the increase in the degree of strain. Strain growth results in the decrease in the number of active glide systems, increasing the shear stress. Combination of these factors results in the Hugoniot elastic limit growth. The measurements were used to draw the Hugoniot elastic limit decay curves and define the power function and plastic yield stresses coefficients for initial and prestrained single-crystal aluminum samples. The spall strength of the single-crystal aluminum is essentially independent on the initial state (degree of prestrain) of samples and depends to a great extent on the sample strain rate before spall fracture. Metallographic analysis of the spall zone on the recovered samples performed by electron microscopy has shown that the aluminum single-crystal fracture is initiated by the initiation of irregularly-shaped micropores that are uniformly distributed across the sample volume independently on the degree of sample strain.

Funding

The study was conducted within R&D № 1770641334821000139O/226/3462-D dated July 22, 2021, and under state assignment AAAA-A19-2021-119071190040 using the equipment provided by the Moscow Regional Explosion Shared Research Center, Russian Academy of Sciences. The samples were prepared under state assignment № 075-00460-21-00 in Joint Institute for High Temperatures, RAS. X-ray diffraction analysis was performed in the Institute of Physics of Metals, Urals branch of RAS (topic „Structure“ № 122021000033-2).

Conflict of interest

The authors declare that they have no conflict of interest.

References

[1] G.T. Gray III, C.E. Morris. J. Physique IV, **01** (C3), 191 (1991). DOI: 10.1051/jp4:1991325
[2] G.T. Gray III, J.C. Huang. Mater. Sci. Eng. A, **145**, 21 (1991). DOI: 10.1016/0921-5093(91)90292-U
[3] J.T. Lloyd, J.D. Clayton, R. Becker, D.L. McDowell. Intern. J. Plasticity, **60**, 118 (2014). DOI: 10.1016/j.ijplas.2014.04.012
[4] G.R. Fowles. J. Appl. Phys., **32**, 1475 (1961). DOI: 10.1063/1.1728382
[5] C.L. Williams, C.Q. Chen, K.T. Ramesh, D.P. Dandekar. J. Appl. Phys., **114**, 093502 (2013). DOI: 10.1063/1.4817844
[6] J.C.F. Millett, N.K. Bourne, M.Q. Chu, I.P. Jones, G.T. Gray, G. Appleby-Thomas. J. Appl. Phys., **108** (7), 073502 (2010). DOI: 10.1063/1.3490135
[7] G.V. Garkushin, G.I. Kanel, A.S. Savinykh, S.V. Razorenov. Int. J. Fract., **197**, 185 (2016). DOI: 10.1007/s10704-016-0074-1
[8] G.D. Owen, D.J. Chapman, G. Whiteman, S.M. Stirk, J.C.F. Millett, S. Johnson. J. Appl. Phys., **122**, 155102 (2017). DOI: 10.1063/1.4999559
[9] G.I. Kanel, S.V. Razorenov, K. Baumung, J. Singer. J. Appl. Phys., **90** (1), 136 (2001). DOI: 10.1063/1.1374478
[10] H. Huang, J.R. Asay. J. Appl. Phys., **100**, 043514 (2006). DOI: 10.1063/1.2266234
[11] H. Huang, J.R. Asay. J. Appl. Phys., **101**, 063550 (2007). DOI: 10.1063/1.2655571
[12] J. Millett, G. Gray III, G. Whiteman, S. Fensin, G. Owen. EPJ Web Conf., **183**, 02010 (2018). DOI: 10.1051/epjconf/201818302010
[13] D.V. Lychagin. Phys. Mesomech., **9** (3), 95 (2006).
[14] L.A. Teplyakova, D.V. Lychagin, I.V. Bespalova. Phiz. mezomekh.**7**, 6 (63) (in Russian).
[15] L.A. Teplyakova, D.V. Lychagin, I.V. Bespalova. Phiz. mezomekh.**9**, 2 (63) (in Russian).
[16] J.C.F. Millett, D.L. Higgins, G. Whiteman, B. Pang, Y.-L. Chiu, I.P. Jones. AIP Conf. Proceed., **1979**, 060004 (2018). DOI: 10.1063/1.5044801
[17] J.C.F. Millett, G. Whiteman, N.T. Park, S. Case, N.K. Bourne. J. Appl. Phys., **113**, 233502 (2013). DOI: 10.1063/1.4810896
[18] E.B. Zaretsky, G.I. Kanel. J. Appl. Phys., **115**, 243502 (2014). DOI: 10.1063/1.4885047

[19] G.I. Kanel, G.V. Garkushin, A.S. Savinykh, S.V. Razorenov, I.V. Paramonova, E.B. Zaretsky. J. Appl. Phys., **131**, 095903 (2022). DOI: 10.1063/5.0082267
[20] G.I. Kanel, G.V. Garkushin, A.S. Savinykh, S.V. Razorenov. J. Experiment. Theore. Phys., **127** (2), 337 (2018). DOI: 10.1134/S1063776118080022
[21] A.S. Savinykh, G.V. Garkushin, S.V. Razorenov. J. Experiment. Theor. Phys., **134** (6) 701 (2022). DOI: 10.1134/S1063776122050053
[22] E.B. Zaretsky, N. Frage, S. Kalabukhov, A.S. Savinykh, G.V. Garkushin, S.V. Razorenov. J. Appl. Phys., **131**, 215905 (2022). DOI: 10.1063/5.0092904
[23] L.M. Barker, R.E. Hollenbach. J. Appl. Phys., **43**, 4669 (1972). DOI: 10.1063/1.1660986
[24] G.K. Williamson, R.E. Smallman. Philosophical Magazine: A J. Theor. Experiment. Appl. Phys., **1** (1), 34 (1956). DOI: 10.1080/14786435608238074
[25] R. Jenkins, R.L. Snyder. *Introduction to X-ray Powder Diffractometry* (John Wiley and Sons, Inc, 1996). DOI: 10.1002/9781118520994
[26] H. Adachi, Y. Miyajima, M. Sato, N. Tsuji. Mater. Transactions, **56** (5), 671 (2015). DOI: 10.2320/matertrans.L-M2015803
[27] S.S. Gorelik, Yu.A. Skakov, L.N. Rastorguev. *Rentgenograficheskiy i elektronno-optichesky analiz* (M., MISIS, 2002) (in Russian).
[28] E.B. Zaretsky, G.I. Kanel. J. Appl. Phys., **112**, 073504 (2012). DOI: 10.1063/1.4755792
[29] R.A. Austin. J. Appl. Phys., **123**, 035103 (2018). DOI: 10.1063/1.5008280
[30] G.I. Kanel, S.V. Razorenov, V.E. Fortov. *Shock-Wave Phenomena and the Properties of Condensed Matter* (Springer, NY., 2004)
[31] G.V. Garkushin G.I. Kanel, S.V. Razorenov. Physics Solid State, **52** (11), 2369 (2010). DOI: 10.1134/S1063783410110247
[32] J.M. Winey, B.M. LaLone, P.B. Trivedi, Y.M. Gupta. J. Appl. Phys., **106**, 073 508 (2009). DOI: 10.1063/1.3236654
[33] T.E. Arvidsson, Y.M. Gupta, G.E. Duvall. J. Appl. Phys., **46**, 4474 (1975). DOI: 10.1063/1.321423
[34] G.I. Kanel. J. Appl. Mechan. Tech. Phys., **42**, 358 (2001). DOI: 10.1023/A:1018804709273
[35] G.I. Kanel, S.V. Razorenov, A.V. Utkin, K. Baumung, H.U. Karov, V. Licht. AIP Conf. Proc., **309** (2) 1043 (1994). DOI: 10.1063/1.46273
[36] J. Belak. J. Computer-Aided Materials Design, **5** (2), 193 (1998). DOI: 10.1023/A:1008685029849

Translated by Ego Translating